Climate and tectonic controls on glaciated critical-taper orogens

Jonathan H. Tomkin [a,*], Gerard H. Roe [b]

[a] *Department of Geology, University of Illinois, Urbana, Il 61801, United States*
[b] *Department of Earth and Space Sciences, University of Washington, Seattle, WA 98103, United States*

Abstract

In this work we present the results of a new analytical model that examines the coupling between glacial erosion and orogen development. Surface processes are assumed to be glacially dominated, and tectonic activity is controlled by critical wedge mechanics. In these circumstances, we find that orogen width is strongly dependent on both the rate of accretion and on the rate of precipitation. The orogen size is linked to tectonic and climate changes via proportionality constants: the orogen width scales with the rate of accretion to between the 2/3rd and 2nd powers, and with the rate of precipitation to the 1/3rd and 5/4th powers. The value of the proportionality constants varies with the taper angle and the relative rates of ice deformation and sliding. In all cases, the sensitivities are higher than those calculated for fluvially-eroding critical wedge orogens. Analytical solutions are supported by the results of a numerical flow-line model. The flow-line model further predicts that uplift rates will be highest at, and just below, the equilibrium line altitude. If glacial ablation is largely a calving process, rock uplift in the wedge will be strongly focused towards the toe. The predicted response time of glaciated orogens to changes in climate and tectonic forcing is dependent upon the constants of erosion, the rheology, and the rate of precipitation. These analyses predict that actual orogens have variable e-folding response times, for example approximately 1.5 Myr for the Southern Alps of New Zealand and the Olympic Mountains of Washington State, and approximately 5.5 Myr for the European Alps.

1. Introduction

Climate plays a fundamental role in determining the topographic evolution of actively uplifting mountain ranges. The consequences of changing rates of precipitation on orogen evolution have been recently considered in models of wedge mechanics (Hilley and Strecker, 2004; Whipple and Meade, 2004; Roe et al., 2006). These models supply explanations of orogen evolution and provide testable predictions for field investigation. Erosion in previous analytical models is restricted to the action of rivers, however, limiting their application. In this study, we present a similar analytical model that is focused on glacially-eroded landscapes.

The role of glaciation in orogen/climate coupling needs to be considered for two reasons. Firstly, glaciers are highly efficient erosive agents. Topography appears to be controlled by glacial extent in a number of places, including the Andes (Porter, 1981), and the Himalaya (Brozovic et al., 1997). Furthermore, glaciated basins produce more sediment per basin area than most fluvial ones (Hallet et al., 1996), indicating that they are more efficient at eroding landscapes. Results from conceptual

* Corresponding author.
E-mail address: tomkin@uiuc.edu (J.H. Tomkin).

(e.g. Whipple and Tucker, 1999) and numerical (e.g., Tomkin and Braun, 2002) models of alpine environments suggest that relief is decreased as glacial coverage increases.

Secondly, most active orogens have been heavily glaciated during the Late Cenozoic (e.g., Denton and Hughes, 1980), including the Himalayas, the Southern Alps of New Zealand, the European Alps, the Andes, the Alaskan Coastal Range, and the Olympic Mountains. All of these ranges also host active glaciers and ice fields today. Describing these systems with fluvial models may therefore be inappropriate for both past and present conditions.

In this study, we find that glacially-eroded, critical-taper orogens (Dahlen, 1984; Dahlen and Barr, 1989; Barr and Dahlen, 1989) behave differently than fluvially-eroded equivalents (Hilley and Strecker, 2004; Whipple and Meade, 2004; Roe et al., 2006). Firstly, the widths of glaciated orogens are predicted to be more sensitive to changes in precipitation rate. For shear-stress based fluvial incision, orogen width scales as precipitation to the $-1/4$ power, while glacial orogen width scales as precipitation to a power between $-1/3$ and $-5/4$. These glacial values are dependent on whether the longitudinal profile of the glacier is more sensitive to internal deformation or to basal sliding, and on the average taper angle of the topography. Secondly, glacial orogens are predicted to have different patterns of erosion and uplift than fluvial orogens. Fluvial erosion models require that rock uplift is fastest in the core of the range (Stolar et al., 2006). In contrast, glacial systems are predicted to have their highest rates of erosion and rock uplift at and below the ablation zone, which are at the edges of the range.

The analytical model is described below. We begin with a simple one-dimensional model of an ice-cap sliding on a flat base, and then examine the significance of internal ice deformation, surface taper angles, and differences in mass balance profiles. A flow-line model is used to extend these results to cases requiring a numerical solution. This numerical solution is also used to predict the response of a few chosen orogens to non-steady conditions. Although we avoid the complications of mixed fluvial–glacial systems in this work, the results presented point the way to a holistic model of climate/orogen coupling that considers the role of temperature, as well as that of precipitation.

2. Analytical model

We seek to determine the scaling relationship between climate, accretionary flux, and orogen width for a glaciated critical-taper wedge. The solution requires modeling the ice profile so as to calculate the glacial erosion yield. As in earlier fluvial studies (Hilley and Strecker, 2004; Whipple and Meade, 2004; Roe et al., 2006), we will examine the system in one dimension. Fig. 1 presents the geometry of the one-sided orogen that we consider initially. The case of a two-sided orogen is examined in the discussion.

The size of the orogen is determined by the balance of accretion and erosion. Wider orogens have larger surface areas available for erosion, and so have higher erosional yields. If accretion outstrips erosion, the orogen will grow until the erosional yield (Y) matches the accretionary flux (F). Conversely, if the erosional yield is larger than the accretionary flux, the orogen will shrink. To compute the mass balance of an orogen we therefore need to describe both the total erosional yield and the accretionary flux.

The accretionary flux is the product of the thickness and velocity of the accreting section. The erosional yield of an orogen, a function of the climate, is not as simply determined. We begin by deriving its value.

As the orogen is ice-covered, glacial erosion is the only long-range erosion process in operation. The physical action of ice on rock is the most important glacial erosion process (as discussed in Hallet et al., 1996), and either abrasion (Boulton, 1979; Hallet, 1979, 1981; Lliboutry, 1994) or quarrying (Hallet, 1996) dominates the glacial erosion yield. Conveniently, both abrasive and quarrying processes can be formulated such that the main control for either mechanism is the ice velocity. In this study we employ a simple, physically justified, erosion model in which the rate of glacial erosion ($\dot{\varepsilon}$) is a function of the ice
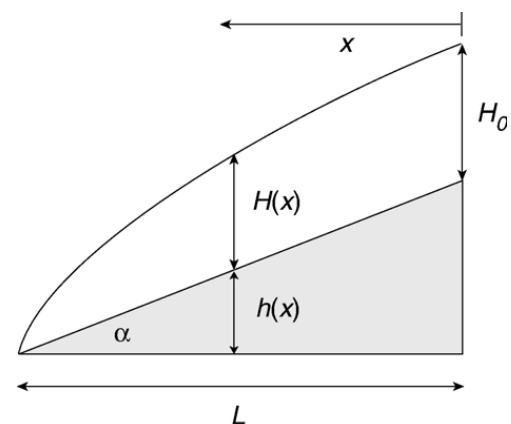

Fig. 1. Schematic of an ice-covered orogen. The taper angle α is controlled by wedge mechanics, while the distribution of ice, $H(x)$, is determined by the physical properties of ice, the pattern of accumulation and ablation, and the width of the wedge, L. The width of the wedge is determined by the balance of erosional and accretionary yield.

sliding velocity (U_s) and is independent of entrained debris:

$$\dot{\varepsilon} = K_g |U_s|^l. \tag{1}$$

where K_g and l are constants. This choice represents the general form of the abrasion law proposed by Hallet (1979) and would apply to any erosion mechanism that scales with basal velocity, including quarrying (Hallet, 1996), and has been used in a number of studies (e.g. Oerlemans, 1984; Harbor et al., 1988; Braun et al., 1999). The available field evidence (Humphrey and Raymond, 1994) suggests that $l = 1$ is valid over 3 to 4 orders of magnitude, and we use that value of l here. Field studies suggest that $K_g = \sim 10^{-4}$ (Humphrey and Raymond, 1994).

The basal sliding velocity, U_s, is described as a function of the ice thickness and slope, as can the depth-integrated deformation velocity ($\overline{U}_d$). From Paterson (1994):

$$|U_s| = f_s H^{n-1} \left| \frac{d(h+H)}{dx} \right|^n \tag{2}$$

$$|\overline{U}_d| = f_d H^{n+1} \left| \frac{d(h+H)}{dx} \right|^n \tag{3}$$

where h is the topographic height, H is the ice thickness, $n = 3$, f_d is a constant, and f_s is also a constant if an average value is used for the sub-glacial water pressure (e.g. Paterson, 1994; Knap et al., 1996).

The glacial erosion rate can therefore be calculated with Eqs. (1) and (2) if the ice profile (Fig. 1) is known. We use the conservation equation to derive the ice profile. The ice thickness, $H(x)$, is a function of distance from the divide, and the total half-width of the orogen is L. $H(x)$ varies from H_0 at the divide to zero at the toe. The orogen has a fixed taper angle, α. To begin with, we consider the case in which precipitation (P) is a constant across the orogen, and ablation is restricted to the toe. In these conditions, we can set up the following conservation equation to describe the ice flux across the orogen:

$$H(|U_s + \overline{U}_d|) = Px. \tag{4}$$

Note the ice thickness H and the sliding and deformation velocities (U_s and $\overline{U}_d$) are functions of x. The left-hand side of Eq. (4) can be rewritten as a function of the ice profile by taking advantage of the fixed topographic slope (Fig. 1), and substituting for the velocities (Eqs. (2) and (3)):

$$H\left(f_d H + \frac{f_s}{H}\right) H^n \left| \frac{d}{dx}\left(H + L \tan \alpha \left(1 - \frac{x}{L}\right)\right) \right|^n = Px. \tag{5}$$

Table 1
Analytically-determined exponents (q and r) linking tectonics and climate in steady-state critical orogens for different slope and ice flow conditions

Topographic slope	Dominant ice flow	General yield relationship $Y \propto P^q L^r$	Width/ climate relationship $L \propto P^{\frac{q}{r}}$	Width/ tectonics relationship $L \propto F^{\frac{1}{r}}$
Low	Deformation	$Y \propto P^{\frac{5}{8}} L^{\frac{1}{2}}$	$L \propto P^{-\frac{5}{4}}$	$L \propto F^2$
Low	Sliding	$Y \propto P^{\frac{5}{6}} L^{\frac{4}{3}}$	$L \propto P^{-\frac{5}{8}}$	$L \propto F^{\frac{3}{4}}$
Low	Mixed	$Y \propto P^{\frac{5}{7}} L^{\frac{6}{7}}$	$L \propto P^{-\frac{5}{6}}$	$L \propto F^{\frac{7}{6}}$
High	Deformation	$Y \propto P^{\frac{2}{5}} L^{\frac{2}{3}}$	$L \propto P^{-\frac{3}{5}}$	$L \propto F^{\frac{3}{2}}$
High	Sliding	$Y \propto P^{\frac{2}{5}} L^{\frac{5}{3}}$	$L \propto P^{-\frac{2}{5}}$	$L \propto F^{\frac{3}{5}}$
High	Mixed	$Y \propto P^{\frac{1}{2}} L^{\frac{3}{2}}$	$L \propto P^{-\frac{1}{3}}$	$L \propto F^{\frac{2}{3}}$

Y is the total erosional yield, P is the precipitation rate, L is the width of the wedge, and F is the accretionary flux. The scale dependence of Y on P is given by the value of q, and the scale dependence of Y on L is given by r.

Eq. (5) has a range of solutions for $H(x)$ that depend on the relative importance of deformation and sliding in determining the ice profile (i.e. the size of $f_d H$ compared to f_s / H), and the basal slope (α).

Once the ice profile is found, then the sliding rate, and thus the rate of glacial erosion, can be determined across the orogen. Table 1 shows the proportionality relationships between the tectonics (accretionary yield), climate (precipitation rate) and the width of the orogen for different topographic slope and ice flow conditions.

We present two examples that illustrate how the results in Table 1 were derived. The other cases listed in Table 1 are solved with analogous methods.

2.1. Example 1: low angled topography, sliding-dominated ice flow

We first present the solution for the limiting case in which the bed has a very low slope ($\alpha \approx 0$) and glacial sliding is much more significant than ice deformation ($f_d H \ll f_s / H$). In this case Eq. (5) can be simplified as

$$f_s H^n \left(\left| \frac{dH}{dx} \right| \right)^n = Px. \tag{6}$$

Eq. (5) can be developed further by non-dimensionalizing the heights and widths, by defining

$$H = H_0 H' \tag{7}$$

and

$$x = Lx'. \tag{8}$$

This gives $\frac{dH}{dx} = \frac{H_0}{L}\frac{dH'}{dx'}$, so Eq. (6) can be expressed as

$$f_s H_0^n H'^n \left(\left\| \frac{H_0}{L}\frac{dH'}{dx'} \right\|\right)^n = PLx' \qquad (9)$$

rearranging Eq. (9) to make the left-hand side of the equation independent of $f_s H_0$, and L gives

$$\frac{H'^n}{x'}\left(\frac{dH'}{dx'}\right)^n = \frac{1}{f_s}\frac{PL^{n+1}}{H_0^{2n}}. \qquad (10)$$

The right-hand side of Eq. (10) is independent of x and thus must be constant. Since f_s is also constant, the combination of H_0, P and L on the right-hand side of Eq. (10) must also be constant. Therefore it can be written that

$$H_0 \propto P^{\frac{1}{2n}}L^{\frac{n+1}{2n}}. \qquad (11)$$

Eq. (11) will be useful shortly.

The rate of erosion across the glacier can also be expressed non-dimensionally. In this case, Eqs. (2), (7) and (8) are substituted into Eq. (1) to give

$$\dot{\varepsilon} = k_g f_s H_0^{n-1} H'^{n-1}\left(\frac{H_0}{L}\frac{dH'}{dx'} + \tan\alpha\right)^n \qquad (12)$$

and as we wish to find the total erosional yield we integrate over the domain:

$$Y = \int_0^L \dot{\varepsilon}\,dx. \qquad (13)$$

Remembering that in this case $\alpha \approx 0$, substituting Eq. (12) into Eq. (13), and removing the dimensional parameters from the integrand produces

$$Y = k_g f_s H_0^{2n-1} L^{1-n} \int_0^1 H'^{n-1}\left(\frac{dH'}{dx'}\right)^n dx'. \qquad (14)$$

The value of the integrand depends upon the boundary conditions of the glacier, but, given those boundary conditions, it is a dimensionless number. Therefore, after subsuming the constants into a proportionality sign, the yield can be expressed as a function of H_0 and L.

$$Y \propto H_0^{2n-1}L^{1-n}. \qquad (15)$$

Finally, we can use Eq. (11) to replace H_0 in Eq. (15):

$$Y \propto P^{\frac{2n-1}{2n}}L^{\frac{3n-1}{2n}}. \qquad (16)$$

Eq. (16) links the yield with the precipitation rate and the width of the orogen. In steady-state flux balance the erosional yield must balance the accretionary flux (i.e., $Y=F$). From Eq. (16):

$$L \propto F^{\frac{2n}{3n-1}}P^{\frac{2n-1}{3n-1}}. \qquad (17)$$

As $n=3$, this suggests that the width of an orogen varies with to the 3/4 power of the accretionary flux and to the 5/8 power of the precipitation rate.

2.2. Example 2: high angle topography, mixed sliding and deformation ice flow

Eq. (17) is the result for a sliding-dominated orogen with a small topographic slope. We will now determine a more complicated case, one in which the ice flows occurs via a mixture of sliding and deformation, and the topographic slope is large ($\frac{H_0}{L}\frac{dH'}{dx'} \ll \tan\alpha$). In this case, Eq. (5) non-dimensionalizes to

$$H_0^{n+1}H'^{n+1}\left(f_a H_0 H' + \frac{f_s}{H_0 H'}\right)\left(\left\|\frac{H_0}{L}\frac{dH'}{dx'}\right\|\right)^n = Px, \qquad (18)$$

which rearranges to

$$\frac{1}{x'}H'^{n+1}\left(f_d H_0 H' + \frac{f_s}{H_0 H'}\right)\tan^n\alpha = \frac{PL}{H_0^{n+1}}. \qquad (19)$$

The right-hand side of Eq. (19) still contains H_0 and so, in contrast to the case of pure sliding, it is not strictly true that the right-hand side of Eq. (19) is constant as the orogen varies. However the two terms within the parentheses on the left-hand side of Eq. (19) will to some extent counteract each other as H_0 varies. We make the simplifying approximation the right-hand side is approximately constant. This assumption is shown to be reasonable in the next section, in which the analytical results are shown to predict the results of a full flow-line calculation.

$$H_0 \propto P^{\frac{1}{n+1}}L^{\frac{1}{n+1}}. \qquad (20)$$

As $\frac{H_0}{L}\frac{dH'}{dx'} \ll \tan\alpha$, Eq. (13) becomes

$$Y = k_g f_s H_0^{n-1} L \int_0^1 H'^{n-1}(\tan\alpha)^n dx'. \qquad (21)$$

Again, the integral is a constant depending only on model boundary conditions and not on the orogen width. Therefore

$$Y \propto H_0^{n-1}L^1. \qquad (22)$$

Substituting Eq. (20) into the integrated yield Eq. (22) and setting $Y=F$ gives

$$F \propto P^{\frac{n-1}{n+1}}L^{\frac{2n}{n+1}}. \qquad (23)$$

Or, in other words:

$$L \propto F^{\frac{n+1}{2n}}P^{\frac{n-1}{2n}}. \qquad (24)$$

This method of analysis can be similarly extended to the other four permutations of taper angles and dominant ice flow regimes. Table 1 summarizes the dependencies between erosional yield, orogen width, tectonic activity, and the rate of precipitation for the different end-member cases.

These analytical results prompt a number of observations concerning glacial erosion and wedge tectonics. Firstly, there is a robust link between the rate of tectonic activity , precipitation, and the width of the orogen: L scales with F in a range of 2/3 to 2, with most dependencies being near-linear or somewhat non-linear (Table 1), and L scales with P in a range of 1/3 to 5/4. Secondly, although orogenic width is more sensitive to the rate of accretion than the rate of precipitation, the values of these scaling dependencies are significant for both. Even the conditions that produce the least sensitive orogen (high slope, mixed ice flow) suggests that width depends on the precipitation rate to the 1/3 power and accretionary flux to the 2/3 power, while more sensitive conditions (such as low slopes and sliding-dominated flow regimes) produce orogens with non-linear (with exponents of 5/4 for the precipitation rate, and 2 for accretionary flux) dependencies between width, precipitation, and the rate of accretion. Thirdly, the glaciated orogen is always more responsive to changes in climate and tectonics than an equivalent fluvially-eroded, orogen (Roe et al., 2006).

These analytical calculations do not predict spatial patterns of erosion and rock uplift, do not specify what angles describe high and low slopes, and do not indicate when ice flow conditions are likely to be mixed or dominated by the sliding or deforming end-members. In the next section, we introduce a flow-line model that explicitly addresses these issues.

3. Flow-line model

In this section, we present the results of a flow-line model that verifies the results of the analytical model and predicts the pattern of erosion across the orogen. In addition, the flow-line model is used to test the significance of glacial isostasy, spatially non-uniform precipitation, and different patterns of ablation in the coupled system.

The flow-line model solves the conservation equation (Eq. (5)) numerically. Finding an ice mass balance solution in this way is not new: an original discussion of this method is presented in Nye (1959), and the technique was first used to calculate erosion rates in Oerlemans (1984). The model we use has been built from textbook techniques (Hutter, 1983, Paterson, 1994). Our flow-line model solves the conservation equation on a desktop computer, with MATLAB's built

in ODE solver (Shampine and Reichelt, 1997). Correctly solving the case in which ablation is restricted to the toe of the glacier requires the use of stretched spatial co-ordinates (as in Roe and Brandon, 2007).

The numerical model is able to solve cases with specific taper angles and spatially variable precipitation and ablation rates. The numerical model is also explicit about the differing contributions of sliding and internal deformation in determining the ice profile, which requires that the values of the velocity parameters f_s and f_d be computed. From Paterson (1994):

$$f_s = \frac{2A_s(\rho g)^n}{0.8} \tag{25}$$

$$f_d = \frac{2A_d}{n+2}(\rho g)^n \tag{26}$$

where A_s is the sliding parameter (which we take to be $1.8 \times 10-16$ Pa^{-3} yr^{-1}m^{-2}), A_d the deformation parameter (which we take to be $2.5 \times 10-16$ Pa^{-3} yr^{-1}), ρ is the ice density (910 kg m^{-3}), g is the acceleration due to gravity, (9.81 m s^{-2}), and the sub-glacial water pressure is 80% of the ice overburden (following Knap et al., 1996). The value of A_d is taken from a review of field data and experimental results by Paterson (1994), and the value of A_s empirically fits the recorded basal velocity of glaciers (Bindschadler, 1983) and agrees with laboratory tests (Budd et al., 1979).

We now present the results of the flow model. We first show an agreement with the scaling ratios determined in the previous section, and then show the pattern of erosion that it predicts for glaciated orogens.

3.1. Verification of scaling relationships

The analytical results (Table 1) restrict the definition of slope angles into two states ("high" and "low") and examine only three ice flow regimes, the two end members (deformation dominated and sliding dominated) and an intermediate mixed case. For the deformation-dominated regime, we assume that the ice profile is determined by the rate of deformation (so $f_s = 0$) but that some sliding (and thus erosion) nevertheless occurs — just not enough to change the shape of the ice profile. The flow-line model is used to solve the conservation Eq. (5) over a range of uniform precipitation rates for a variety of topographic slopes. In this way, the scaling predictions of the analytical model can be compared against specific taper angles.

Fig. 2 shows the dependence of orogen width on precipitation rate (q) and the accretionary flux (r), as determined from the numerical model (grey shapes) and
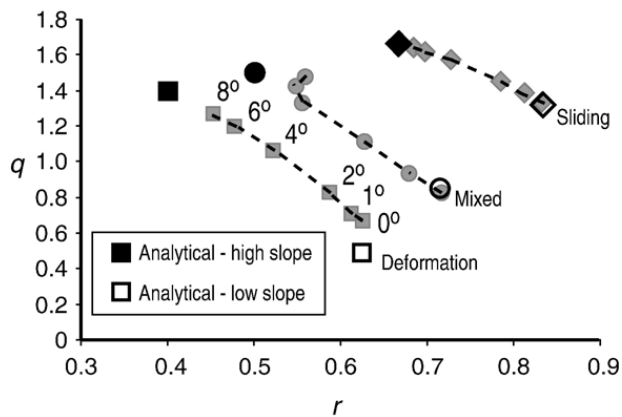
Fig. 2. Analytically- and numerically-determined power dependencies (q and r) of the orogen width on the rate of precipitation and the accretionary yield. Ice profiles determined purely by deformation (squares), purely by sliding (diamonds), and by a mixture of both (circles) produce different solutions. Unshaded shapes indicate analytical "low" slope values, black shapes indicate analytical "high" slope values (from Table 1), and numerical values (from 0 to 8°, linked in order by the dashed line) are shown in grey. Note that the analytical solutions provide lower and upper bounds on the numerical results: increasing the finite slope moves the solution from the "low" analytical result towards the "high" analytic result. This relationship is most exact for the pure sliding case. The small deviations from this trend for the deforming and mixed cases are a consequence of the approximation made in Eq. (20).

predicted by the analytical model (unshaded and black shapes). The "low" slope results reproduce the flow-line model solution when the topography is flat ($\alpha = 0$). A critical-taper angle of 8° in the flow-line model closely approximates the analytical model's prediction for "high" taper angles. Taper angles between 0° and 8° have scaling dependencies that are linear mixes of the analytically determined "low" and "high" results. As the angle increases from zero the dependencies become increasingly weighted towards the "high" slope result.

Including the isostatic effect of the ice on the orogen in the flow-line model lowers the surface topography slightly, creating a non-uniform basal slope, but does not significantly alter the scaling relationships shown in Fig. 2.

3.2. Connection between erosion yield and slope

High taper angles increase the surface slope of the ice, thus increasing the basal shear stress and the rate of erosion. The erosional yield is therefore related to the taper angle (Fig. 3). For taper angles near zero this relationship is weak, as ice flow mechanics has the greatest influence on the ice profile. At taper angles greater than about 4°, however, the ice surface slope is largely determined by the taper slope. At these higher taper angles the erosional yield is a power function of the taper angle (Fig. 3).

For any given angle, sliding-dominated ice profiles produce higher erosional yields than deformation-dominated ice profiles (Fig. 3). Sliding-dominated ice profiles are thicker than deformation-dominated profiles, as the latter is more efficient at transporting the ice flux resulting from precipitation. As ice thickness increases, so does the shear stress at the base, which equates to higher rates of erosion. As the two flow regimes are additive the mixed case has the thinnest ice profile and the lowest erosional yield.

3.3. Pattern of erosion

The flow-line model predicts the spatial pattern of the erosion rate. As the topography is in steady-state, erosion rates are equivalent to rock uplift rates. The distribution of rock uplift is sensitive to both the climate and the slope of the wedge. For typical orogenic slopes, erosion rates (and therefore rock uplift rates) are higher towards the edge of the orogen. The gradient in erosion rates is determined by the ablation pattern: it is most pronounced if ablation is dominated by ice calving at the glacial toe and less pronounced if ablation is controlled by melting rates. In either case, erosion rates are highest at and below the equilibrium line altitude.

Typical orogenic wedges have surface slopes of between 2 (e.g. Barbados: Westbrook et al., 1988) and 6° (e.g. Taiwan/Olympics: Davis et al., 1983). Fig. 4 illustrates the influence of orogenic slope on the modeled pattern of erosion. For Coulomb-plastic wedges, the slope is controlled by the crust rheology, and is a constant regardless of the size of the orogen. In this figure, the ice
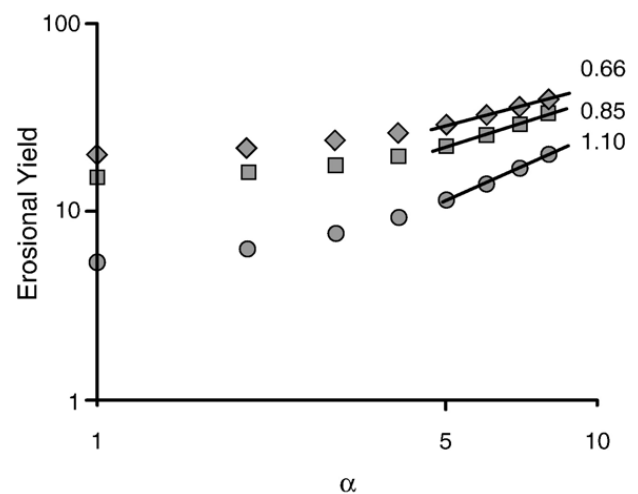

Fig. 3. Log–log plot of erosional yield versus slope for ice profiles that are the result of pure deformation (grey squares), pure sliding (diamonds), and a mixture of the two (grey circles), calculated from the numerical flow-line model. Black lines indicate linear fits for high angled (above 4°) slopes. The slopes of the linear fits are indicated for each of the three cases.
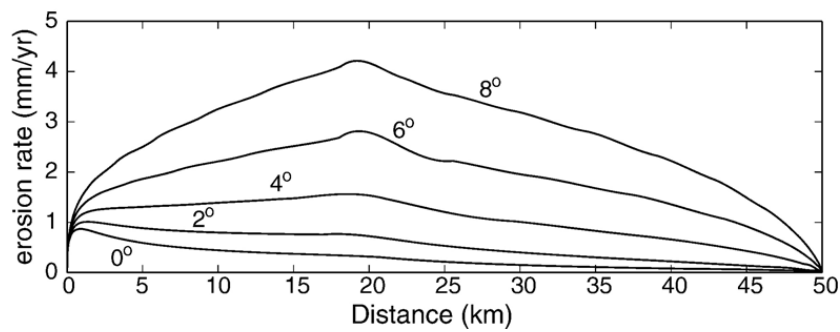
Fig. 4. Erosion rate patterns across the orogen for different taper angles. The ice profiles that produce these patterns are the result of mixed sliding and deformation, with an accumulation zone that covers the upper 60% of the orogen (between 20 and 50 km), below which uniform ablation occurs such that ice flux goes to zero at the glacial snout.

profile is determined by the mixed case, with flow rates determined by Eqs. (25) and (26). The accumulation zone occurs over the upper two thirds of the orogen, balanced by ablation over the lower third. Orogens with low slopes (below 4°) have their highest erosion rates in the ablation zone. Erosion rates in the ablation zone are roughly twice as high as those in the accumulation zone. In orogens with higher slopes (above 4°), the erosion yield increases, and the erosion rate peaks at the equilibrium line altitude, in line with previous expectations (Andrews, 1972; Hallet, 1979). The erosion rate is somewhat symmetrical around the equilibrium line altitude for high-sloped orogens, but

as the ablation zone is shorter than the accumulation zone, the lower part of the orogen experiences a higher average ice flux and so erosion rates are still somewhat higher towards the toe. The small, higher frequency variations in the modeled erosion rate are the result of slight numerical instabilities in the solution.

The pattern of erosion is strongly controlled by the distribution of accumulation and ablation. This is demonstrated by changing the position of a step function between accumulation and ablation. Four different cases are shown in Fig. 5, in which the slope is held constant at 5° while the ablation/accumulation pattern is
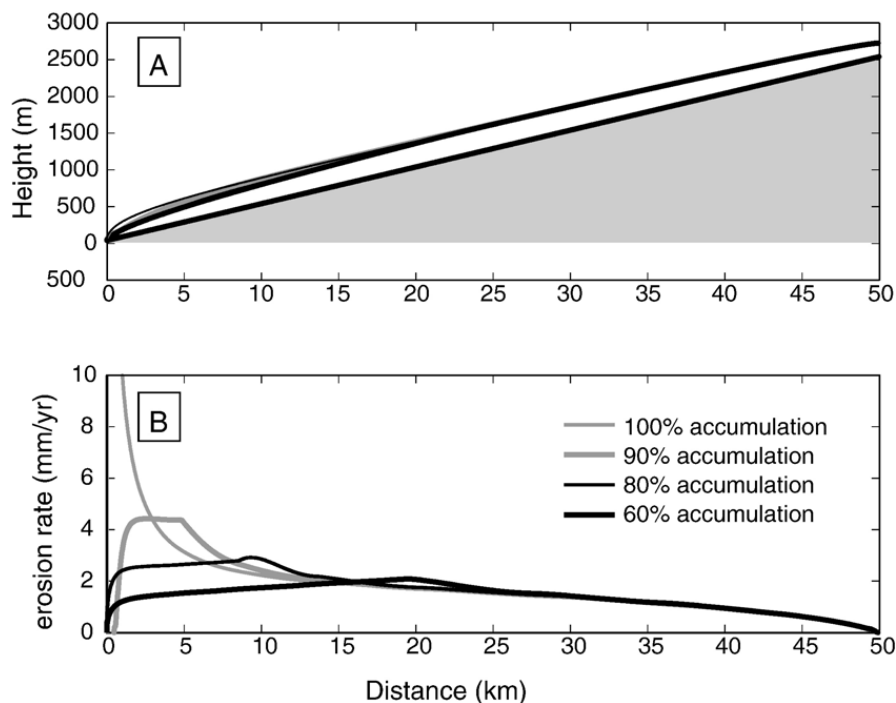

Fig. 5. Ice profile (A) and erosion rate (B) across the orogen for different accumulation/ablation ratios. The taper angle is fixed at 5°. In (A), the orogen itself is indicated by the shaded grey region. The different ice profiles are indicated by the thin grey line (100% accumulation across the orogen), thick grey line (90% accumulation), thin black line (80% accumulation), and thick black line (70% accumulation). The percentages indicate the size of the accumulation zone as a proportion of the entire orogen. Note that all four accumulation functions produce similar ice profiles (upper figure) but dissimilar erosion patterns. The highest rate of erosion occurs at the point of maximum flux (at which the ablation function replaces the accumulation function): the equilibrium line altitude (ELA). Erosion rates remain relatively higher below the ELA than above it; most of the rock uplift in a steady-state wedge is near the toe.

changed. In all cases, the accumulation zone is described by a uniform 1 m/yr rate of (ice thickness equivalent) precipitation. This accumulation zone begins at the divide and continues for a proscribed distance downslope. Below the accumulation zone there is a zone of uniform ablation, the magnitude of which is chosen such that the sum of ice ablated equals the sum of ice accumulated. Ablation rates are thus faster for smaller ablation zones. In the case of 100% accumulation, ablation is infinite over an infinitesimal distance at the toe; this is the end-member case in which all ablation is the result of calving. The other end-member occurs when the ablation/accumulation proportion is 40/60, which is the maximum average size of the accumulation area ratio observed in nature (Porter, 1979; Meierding, 1982). Note also that the total accumulation, and thus the ice flux, is larger when the equilibrium line altitude is lower. As a consequence, the total erosional yield is also larger when the equilibrium line altitude is lower.

4. Discussion

4.1. Orogen uplift pattern comparison

The observed behavior of actual orogens provides some support for the tectonic uplift dependence on climate described here. Although currently available data is open to different interpretations, it is hoped that this work suggests a way of testing different hypothesis for the evolution of specific orogens. We describe how the predicted pattern of rock uplift is consistent with observations from the Southern Alps, the Chugach/St Elias mountains of Alaska, and the Olympic Mountains of Washington State.

The model predicts that rock uplift rates should be linked to the distribution of precipitation, as observed in the Southern Alps of New Zealand. The Southern Alps is an active mountain range that was covered by an icecap at the LGM (Denton and Hughes, 1980). The rock uplift rate and topographic maxima do not coincide; uplift rates are highest on the western flank of the range (Kamp and Tippett, 1993). Reconstructions of the glacial coverage at the LGM (Soons, 1979) suggest that the strong precipitation gradient across the range (Griffiths and McSaveney, 1983) depressed the ELA by several hundred meters on the western side. This suggests increased glacial erosion rates on the western flank relative to the center of the range and the eastern flank. Both rock uplift rates and precipitation rates are around five times higher on the western flank, which is consistent with rock uplift rates being approximately linearly related to the precipitation rate (Table 1).

Modeled patterns of long-term rock uplift are dependent on ice flux: high rock uplift rates are associated with high rates of precipitation and restricted regions of ablation. This is consistent with observations made in the Chugach/St. Elias Range of southern Alaska, where long-term rock uplift rates appear to be controlled by the rate of ice accumulation (Meigs and Sauber, 2000). A combination of increased coastal precipitation and a spatially-varying lapse rate have strongly depressed the ELA on the western side of the range relative to the eastern side (Pewe, 1975). Calculated sediment flux (Hallet et al., 1996) and fission track data (O'Sullivan et al., 1997) from the region support the view that rock uplift rates are higher in the western and central parts of the range than on the eastern side.

The model requires that rock uplift rates are highest in the glaciated portion of mixed-process orogens. This is observed in the Olympic Mountains of Washington State, where rock uplift rates are spatially non-uniform and biased toward high elevations (Pazzaglia and Brandon, 2001). The Olympics represent the exposed crest of the accretionary complex of the Juan de Fuca subduction zone, and fission-track ages from zircons indicate that the Olympics have been actively exhuming since at least 14 Ma (Brandon et al., 1998). These zircon fission track ages, together with apatite fission track ages and apatite He ages consistently show the highest rates of exhumation ($\sim$ 1 mm/yr) in the core of the range, with significantly lower values ($\sim$ 0.1 mm/yr) on the flanks. The range was glaciated by a local ice sheet at the last glacial maxima that was largely restricted to the center of the range (Heusser, 1974; Thackray, 2001): the regions of intensive glaciation and high rock uplift rate substantially overlap. This suggests the possibility that the pattern of rock uplift in the range is glacially controlled. However, Stolar et al. (2006) note that higher uplift rates in the core of the range might also be expected for fluvially controlled systems. As the Olympics is a mixed fluvial/glacial system, more detailed modeling is required to resolve the relative importance of the different surface processes.

4.2. Two-sided critical wedge

The analytical and numerical results presented above describe the behavior of a one-sided critical wedge. A single-sided critical wedge description is probably reasonable for many glaciated orogens. The analytical results (Table 1) indicate that erosional yields are sensitive to the precipitation rate. Precipitation rates are usually substantially higher on one side of an orogen (e.g. Soons, 1979; Hulton et al., 1994; Thackray, 2001) than the other. Erosional yields are therefore likely dominated by the windward side of the range. Furthermore, as

we show in this section, the dependencies of a one-sided wedge bound any two-sided solution.

Two sided critical wedges are made up of a pro-side, where material is accreted, and a retro-side (Willett et al., 1993). Two-sided wedges are similar to one-sided wedges, in that they grow self-similarly, but the slopes of the two sides can differ with the retro-side being steeper (Dahlen, 1984). If the slopes are different on either side of the central divide, erosion rates, and thus uplift rates, can also be different, leading to an uneven partitioning of rock uplift rates across the two sides of the orogen. Previous analytical models have examined this partitioning for a two-sided orogen that is fluvially-eroded (Whipple and Meade, 2004; Roe et al., 2006), finding that the steeper sloped retro-side experiences higher rates of rock uplift than the pro-side, regardless of the rates of precipitation or tectonic accretion. The glacial case is more complicated, as the taper angle partly determines how the erosional yield varies with the rate of precipitation.

We begin by stating the general yield equation for each side of the orogen. Generalizing Eq. (16), and denoting subscripts of p for the pro-side and ψ for the retro-side gives:

$$Y_{\mathrm{p}} = k_p P_p^{qp} L_p^{rp} \qquad (27a)$$

$$Y_\psi = k_\psi P_\psi^{q\psi} L_\psi^{r\psi} \qquad (27b)$$

where k_p and k_ψ are constants. Total erosional yield Y is a sum of the pro- and retro-side yields ($Y = Y_\mathrm{p} + Y_\psi$).

If the two sides have the same slope, then the equivalent constants and exponents (k_p and k_ψ, q_p and q_ψ, r_p and r_ψ) in Eqs. (27a) and (27b) will have identical values. In this case, if precipitation is constant across the range, erosional yield will be equally partitioned to the pro- and retro-sides. If the pro- and retro-slopes are not equal, however, each side will have different dependencies.

Consider the case in which a sliding-dominated glacier covers a two sided wedge in which the pro-side has a "low" slope and the retro-side a "high" one. Using Table 1 and Eqs. (27a) and (27b), we find that

$$Y_p = k_p P_p^{5/6} L_p^{4/3} \qquad (28a)$$

$$Y_\psi = k_\psi P_\psi^{2/3} L_\psi^{5/3}. \qquad (28b)$$

Here, the pro-side yield is more sensitive than the retro-side yield to changes in precipitation, but less sensitive to changes in width. Table 1 reveals that this trend is the same for all three types of ice flow. Increasing a uniform precipitation rate (i.e., $P_\mathrm{p} = P_\psi$), for example, increases the yield of the (low sloped) pro-side relative to the (high sloped) retro-side. This indicates that even though $k_\mathrm{p} < k_\psi$ (note the positive relationship between taper angle and erosional yield when all else is held constant, Fig. 3), the side of the wedge that produces the highest erosional yield depends on the climatic and tectonic conditions.

Eqs. (28a) and (28b) indicate that different sides of the wedge may have different climate and tectonic dependencies. It follows that a two-sided wedge may not have the same r and q exponents as a one sided wedge. The dependency is bound by the one-sided solutions however: in the sliding-dominated case the effective value of q is between 2/3 and 5/6 (Eqs. (28a) and (28b)), for example, regardless of the values of the constants and exponents. If one side of the wedge is much more erosive than the other the flux equation collapses to the one-sided wedge case (where $F = Y_p$ or $F = Y_\psi$), as do the climate and tectonic dependencies.

4.3. Temperature/tectonic coupling and the glacial buzzsaw

We have examined the role of precipitation in orogen control, but if glacial erosion is the dominant erosion process, another climate parameter – temperature – is the ultimate control. The empirical evidence (Porter, 1981; Brozovic et al., 1997) for glacial erosion's significant influence on surface evolution comes from the coincidence between summit elevations and the glacial equilibrium line altitude (ELA). This accord along many mountain ranges implies that glaciers limit topography to a maximum elevation near the ELA, the so-called "glacial buzzsaw hypothesis". The scaling relationships produced (Fig. 2) by the sliding based erosion model suggests a physical basis for this observation in critical-taper orogens.

The scaling relationships of Table 1 do not require that the entire orogen be glaciated; only that glaciers are the predominant agent of erosion. In the absence of other significant erosion processes, the total rock uplift rate can be balanced by a glacial erosion rate that is restricted to higher alpine regions. The total erosional yield in this case is roughly linearly proportional to the glacial extent (exponent r, Table 1 and Fig. 2). Given a constant lapse rate and precipitation rate, the ELA is controlled by the mean sea-level temperature. If a cooling climate reduces the sea-level temperature, the ELA drops, and the area of glacial extent increases. Increasing the glacial extent increases the erosional yield, so the orogen decreases in size as erosion outpaces accretion. As the orogen shrinks, the area of glacial coverage also decreases. Eventually, the area of glacial coverage will return to its original, pre-

climate change area. The erosion yield once again matches the accretionary yield, and a new steady-state orogen width is reached. The topography is now lower, however, and its maximum height was determined by the change in sea-level temperature, as predicted by the glacial buzzsaw hypothesis.

4.4. The response time of glaciated orogens to tectonic or climate change

We have previously discussed how orogen width is sensitive to the precipitation rate and accretionary flux (Table 1). If there is a change in either tectonic or climate regimes it is possible to predict the future steady-state orogen width and rock uplift rate profile. The orogen will evolve toward this new steady-state. We have not yet determined the time needed for the orogen to reach this new steady-state, however. In this section, we show how the response time of an orogen to a step function in tectonic or climate forcing is dependent on both the properties of the wedge and on the precipitation rate.

If an initially steady-state orogen experiences a change in either the precipitation rate or accretionary flux, the width of the orogen will adjust until erosion once again balances accretion. The area of the orogen A changes with time if there is an imbalance between the incoming tectonic flux F and the erosional yield Y. Table 1 indicates that the erosion yield obeys the general relationship $Y = k_1 P^r L^q$. We can therefore state:

$$\frac{dA}{dt} = F - k_1 P^r L^q. \tag{29}$$

Note that the orogen area is a function of the orogen width: $A = DL/2$ where D is the total wedge thickness. If the orogen is isostatically balanced, the total thickness is a function of the height, H, and the crust, ρ_c, and mantle, ρ_m, densities: $D = H/(1 - \rho_c/\rho_m)$. As the orogen height is also a function of the length, we can rewrite Eq. (29) as

$$\frac{dA}{dt} = F - k_1 k_2 P^r A^{\frac{q}{2}} \tag{30}$$

where $k_2 = \sqrt{(1 - \rho_c/\rho_m)/\tan\alpha}$. In general, Eq. (30) does not have an analytical solution. However, $0 < q/2 < 1$, (from Table 1) and thus it is possible to bound the time response to be between the two end-members, where $\lambda = k_1 k_2 P^r$ and t is the time since the change in system forcing:

$$A(t) = A_f + (F - \lambda)t \quad \text{for } q/2 \rightarrow 0 \tag{31a}$$

$$A(t) = A_f + (A_i - A_f)e^{-\lambda t} \quad \text{for } q/2 \rightarrow 1. \tag{31b}$$

The solution to the time response is bound by these two curves — Fig. 6's shaded region indicates the possible change in area over time for an orogen that grows from one steady-state area A_i to another, A_f.

Note that in this case the e-folding response time is dependent on the taper angle ($\lambda \propto \alpha^{-1/2}$ for small angles) and the precipitation rate ($\lambda \propto P^r$).

4.5. Approximate response times for actual orogens

The previous analysis can be used to predict the timeframe over which specific orogens react to tectonic and climate change. We examine three different active orogens that have all been substantially glaciated during the Late Cenozoic, and all host active glaciers today: the European Alps, the Southern Alps of New Zealand, and the Olympic Mountains of Washington State. We calculate the approximate response time of the orogens numerically. The results should be treated somewhat cautiously, however, as they rely on modern observations of tectonic fluxes and climate, and represent these complex orogens as one-dimensional wedges that are glacially dominated.

To calculate the mass balance for a particular orogen, we need to determine both the accretionary flux and the total erosional yield. The accretionary flux is the product of the accreting thickness and the rate of accretion: it has been estimated to be 75 m²/yr for the European Alps and 52 m²/yr for the Olympic Mountains (Brandon, 2004). The Southern Alps is more complicated (as rates of accretion vary across the orogen, and the thickness of accretion is poorly constrained) but appears to be very large, perhaps as much as 300 m²/yr (using values described in Batt and Braun, 1999).
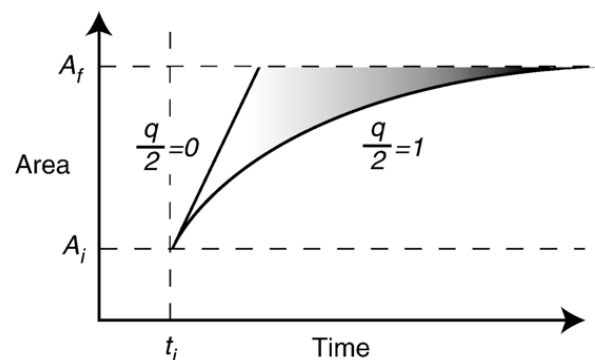

Fig. 6. Area versus time for a non-steady-state, glaciated, orogen. The grey region marks the solution space for any evolution curve that begins at (t_i, A_i) and then asymptotes to the line A_f. Regardless of the system characteristics (such as taper angle, ice flow characteristics, or precipitation rate) the curve is bound by the lines created by Eqs. (31a) ($q/2 = 0$) and (31b) ($q/2 = 1$).

The erosional yield is determined by substituting Eq. (1) into Eq. (13), and requires estimates of the surface taper angle and the rate of precipitation. We assume here that all three orogens experience a mixed deformation/sliding regime. The taper angle is smallest in the European Alps (∼2°) and larger for the Olympics (∼4°) and Southern Alps (∼6°) (Pfiffner et al., 1997; Willett, 1999). Precipitation rate also varies greatly, from ∼1.5 m/yr in the European Alps (Frie and Schar, 1998), to ∼3 m/yr in the Olympics (Anders et al., in press), and ∼10 m/yr in the Southern Alps (Griffiths and McSaveney, 1983).

Different steady-state widths that match erosional yield with the accretionary flux are predicted for each range considered as a single sided wedge. Encouragingly, this simple model predicts reasonable steady-state widths of glaciation (65 km for the European Alps, 49 km for the Southern Alps, and 21 km for the Olympic Mountains) for the standard value of the glacial erosion constant ($K_g = 10^{-4}$). In these examples, ice accumulation occurs in the upper two thirds of the orogen while the lower third ablates. The orogen width is sensitive to this accumulation/ablation function: restricting ablation to the toe of the glacier more than doubles the erosional yield, for example.

By normalizing the length scale of the different orogens, we can compare their time response. As an example, we set the initial width of the orogen so that the erosional yield is 75% of that required to balance the incoming flux. The orogen therefore needs to increase in width so that the erosion yield matches the accretionary flux and steady-state is achieved. This change over time is illustrated in Fig. 7. As can be seen, the Southern Alps and the Olympics require approximately the same amount of time to approach a steady-state, while the European Alps

require substantially more time. The European Alps are slower to respond because of the orogens' large volume. The higher accretionary flux of the Southern Alps relative to the Olympic Mountains compensates for the Southern Alps larger volume, so the two orogens have coincidentally similar response times.

These response times can be quantified. As these curves are approximately exponential in form, we can use the e-folding time to characterize the time response of different orogens. The Olympics have an e-folding time of ∼1.5 Myr, the Southern Alps of New Zealand also have an e-folding time of ∼1.5 Myr, and the European Alps have a longer e-folding time, of ∼5.5 Myr.

This e-folding time has consequences for orogen evolution. Firstly, short term climate fluctuations, such as Milankovitch cycles, will get averaged, and will not affect orogen-scale dynamics. Although such glacial cycles can influence the surface geomorphology, they do not persist long enough to induce variations in the orogen size. The longer-term cooling over the Late Cenozoic, which occurs at the million year time scale, should induce changes in orogen width and rock uplift rates, however.

Secondly, the e-folding times are significantly shorter than the life of the orogens themselves: the Olympics are about 15 Myr old (Brandon, 2004), the European Alps ∼50 Myr (Brandon, 2004), and the Southern Alps ∼5 Myr (Batt and Braun, 1999). This indicates that climate change does have the capacity to influence the evolution of orogens and that these changes may be observed in rock uplift records at Myr timescales.

Finally, it is interesting to note that these estimates for e-folding times are similar to an estimate for a fluvially-dominated orogen. The Central Range of Taiwan (which was largely unglaciated during the LGM) has been modeled as a fluvially-controlled orogen by Whipple and Meade (2006), and they predict that its e-folding time is ∼1.2 Myr. Glaciated orogen responses should be easier to detect, however, as the size of the response to changes in climate and tectonics is predicted to be significantly larger.

5. Conclusions

We have modeled an orogen in which glaciers are the dominant erosive process and tectonic uplift is controlled by critical-taper mechanics. There are some similarities with the results of previous studies (Hilley and Strecker, 2004; Whipple and Meade, 2004; Roe et al., 2006) in which fluvial erosion is the dominant erosive process. The sensitivity of orogen width to precipitation rate for both glacially and fluvially-eroding critical wedges supports the idea of climate/tectonic coupling. In both cases, the mean rate of rock uplift across the orogen is
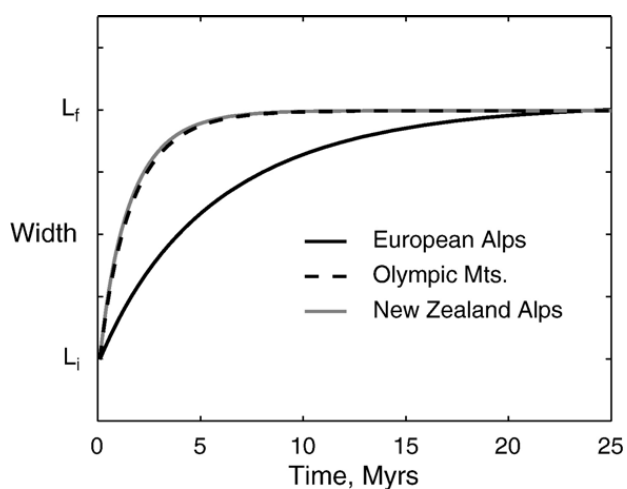

Fig. 7. Dimensionless orogen width versus time for the European Alps, the Olympic Mountains of Washington State, and the Southern Alps of New Zealand. L_f is set to be the steady-state width for each of the orogens, and $L_i = 0.75 \times L_f$.

directly tied to the orogenic width, so changes in rock uplift rates are linked with changes in climate.

Glacially-dominated orogen widths are predicted to be more sensitive to both tectonic and climatic changes than fluvially-dominated orogens. The smallest sensitivity to precipitation (with an exponent of $-1/3$), and the smallest sensitivity to accretionary flux (with an exponent of 2/3) determined for the glacial orogen case are larger than those predicted for the shear-stress fluvial case (with equivalent exponents of $-1/4$ and 1/2, respectively, e.g. Roe et al., 2006). In some circumstances, width scaling is super-linear for the glaciated case: the largest precipitation rate sensitivity is $-5/4$, and the largest accretionary rate sensitivity is 2.

Rock uplift rate in glacially-dominated wedges is predicted to have a spatial pattern controlled by the climate. Rock uplift rates are predicted to be highest at, and just below, the ELA, which is controlled by temperature, precipitation, and the ablation mechanism. Lowering the ELA by lowering the mean annual temperature is predicted to increase rock uplift rates at the toe of the orogen.

Initial estimates of the response times of glaciated orogen are also presented in this work. Approximate calculations indicate that glaciated orogens tectonically respond to changes in climate forcing and accretionary fluxes at million year time scales, with e-folding times calculated for the Southern Alps of New Zealand and the Olympic Mountains of Washington State to be ~ 1.5 Myr, and the e-folding time of the European Alps calculated to be ~ 5.5 My. This response time is similar in magnitude to changes in climate that have occurred over the Late Cenozoic, and we predict that evidence of climate/tectonic coupling can be found via thermochronologic dating techniques.

Acknowledgments

References

Anders, A.M., Roe, G.H., Durran, D.R., and J.R., Minder, in press. Small-scale spatial gradients in climatalogical precipitation on the Olympic Peninsula. J. Hydrometeorol.

Andrews, J.T., 1972. Glacier power, mass balances, velocities and erosion potential. Z. Geomorphol. N.F. Suppl. Bd. 13, 1–17.

Barr, T.D., Dahlen, F.A., 1989. Brittle frictional mountain building: 2. Thermal structure and heat budget. J. Geophys. Res. 94, 3923–3947.

Batt, G.E., Braun, J., 1999. The tectonic evolution of the Southern Alps, New Zealand: insights from fully thermally coupled dynamical modelling. Geophys. J. Int. 136, 403–420.

Bindschadler, R., 1983. The importance of pressurized subglacial water in separation and sliding at the glacier bed. J. Glaciol. 29, 3–19.

Boulton, G.S., 1979. Processes of glacial erosion on different substrata. J. Glaciol. 23, 15–38.

Brandon, M.T., 2004. The Cascadia subduction wedge: the role of accretion, uplift, and erosion, In: van der Pluijm, B.A., Marshak, S. (Eds.), 2nd edition. Earth Structure, An Introduction to Structural Geology and Tectonics. WCB/McGraw Hill Press, pp. 566–574.

Brandon, M.T., Roden-Tice, M.K., Garver, J.I., 1998. Late Cenozoic exhumation of the Cascadia accretionary wedge in the Olympic Mountains, northwest Washington State. Geol. Soc. Amer. Bull. 110, 985–1009.

Braun, J., Zwartz, D., Tomkin, J.H., 1999. A new surface processes model combining glacial and fluvial erosion. Ann. Glaciol. 28, 282–290.

Brozovic, N., Burbank, D., Meigs, A., 1997. Climatic limits on landscape development in the northwestern Himalaya. Science 276, 571–574.

Budd, W.F., Keage, P.L., Blundy, N.A., 1979. Empirical studies of ice sliding. J. Glaciol. 23, 157–170.

Dahlen, F.A., 1984. Non-cohesive critical coulomb wedges: an exact solution. J. Geophys. Res. 89, 10125–10133.

Dahlen, F., Barr, T., 1989. Brittle frictional mountain building: 1. Deformation and mechanical energy budget. J. Geophys. Res. 94, 3906–3922.

Davis, D., Suppe, J., Dahlen, F.A., 1983. Mechanics of fold-and-thrust belts and accretionary wedges. J. Geophys. Res. 88, 1153–1172.

Denton, G.H., Hughes, T.J., 1980. The Last Great Ice Sheets. Wiley, New York. 484 pp.

Frie, C., Schar, C., 1998. A precipitation climatology of the Alps from high-resolution rain-gauge observations. Int. J. Climatol. 18, 873–900.

Griffiths, G.A., McSaveney, M.J., 1983. Distribution of mean annual precipitation across some steepland regions of New Zealand. N.Z. J. Sci. 26, 197–208.

Hallet, B., 1979. A theoretical model of glacial abrasion. J. Glaciol. 17, 209–222.

Hallet, B., 1981. Glacial abrasion and sliding: their dependence on the debris concentration in basal ice. Ann. Glaciol. 2, 23–28.

Hallet, B., 1996. Glacial quarrying: a simple theoretical model. Ann. Glaciol. 22, 1–8.

Hallet, B., Hunter, I., Bogen, J., 1996. Rates of erosion and sediment evacuation by glaciers: a review of field data and their implications. Glob. Planet. Change 12, 213–235.

Harbor, J.M., Hallet, B., Raymond, C.F., 1988. A numerical model of landform development by glacial erosion. Nature 333, 347–349.

Heusser, C.J., 1974. Quaternary vegetation, climate, and glaciation of the Hoh river valley, Washington. Geol. Soc. Amer. Bull. 85, 1547–1560.

Hilley, G.E., Strecker, M., 2004. Steady state erosion of critical Coulomb wedges with applications to Taiwan and the Himalaya. J. Geophys. Res. 109. doi:10.1029/2002JB002284.

Hulton, N., Sugden, D., Payne, A., Clapperton, C., 1994. Glacier modeling and the climate of Patagonia during the last glacial maximum. Quat. Res. 42, 1–19.

Humphrey, N.F., Raymond, C.F., 1994. Hydrology, erosion and sediment production in a surging glacier: Variegated Glacier, Alaska, 1982–83. J. Glaciol. 40, 539–552.

Hutter, K., 1983. Theoretical Glaciology. Riedel, Dordrecht. 510 pp.

Kamp, P.J, Tippett, J.M., 1993. Dynamics of Pacific Plate Crust in the South Island (New Zealand) zone of oblique continent–continent convergence. J. Geophys. Res. 98, 16,105–16,118.

Knap, W., Oerlemans, J., Cadee, M., 1996. Climate sensitivity of the ice cap of King George Island, South Shetland Islands, Antarctica. Ann. Glaciol. 23, 154–159.

Lliboutry, L.A., 1994. Monolithologic erosion of hard beds by temperate glaciers. J. Glaciol. 40, 433–450.

Meierding, T.C., 1982. Late Pleistocene glacial equilibrium line altitudes in the Colorado Front Range: a comparison of methods. Quat. Res. 18, 289–310.

Meigs, A., Sauber, J., 2000. Southern Alaska as an example of the long-term consequences of mountain building under the influence of glaciers. Quat. Sci. Rev. 19, 1543–1562.

Nye, J.F., 1959. The motion of ice sheets and glaciers. J. Glaciol. 3, 493–507.

Oerlemans, J., 1984. Numerical experiments of large scale glacial erosion. Z. Gletsch.kd. Glazialgeol. 20, 107–126.

O'Sullivan, P.B., Plafker, G., Murphy, J.M., 1997. Apatite fission-track thermotectonic history of crystalline rocks in the northern St. Elias Mountains, Alaska. In: Domouling, J.A., Gray, J.E. (Eds.), Geological Studies in Alaska by the U.S. Geological Survey, 1995. United States Geological Survey, Reston, pp. 283–293.

Paterson, W.S.B., 1994. The Physics of Glaciers, 3rd edition. Pergamon. 480 pp.

Pazzaglia, F.J., Brandon, M.T., 2001. A fluvial record of long-term steady-state uplift and erosion across the Cascadia forearc high, western Washington State. Am. J. Sci. 301, 385–431.

Pewe, T.L., 1975. Quaternary Geology of Alaska. United States Geological Survey Professional Paper. 145 pp.

Pfiffner, O.A., Erard, P.F., Stuble, M., 1997. Two cross sections through the Swiss Molasse Basin. In: P¢¡ner, O.A., Lehner, P., Heitzmann, P., Mueller, St., Steck, A. (Eds.), Deep Structure of the Swiss Alps: Results of NRP20. Birkh userVerlag, Basel, pp. 64–72.

Porter, S.C., 1979. Hawaiian glacial ages. Quat. Res. 12, 161–187.

Porter, S.C., 1981. Pleistocene glaciation in the southern Lake District of Chile. Quat. Res. 16, 263–292.

Roe, G.H., Stolar, D.S., Willett, S.D., 2006. Response of a steady-state critical wedge orogen to changes in climate and tectonic forcing. Geol. Soc. Amer. 398, 227–239 (Special paper).

Roe, G.H., and M.T. Brandon, 2007. Critical form and feedbacks in mountain belt dynamics: the role of rheology (in submission).

Soons, J.M, 1979. Late Quaternary environments in the central South Island of New Zealand. N.Z. Geogr. 35, 16–23.

Shampine, L.F., Reichelt, M.W., 1997. The MATLAB ODE suite. SIAM J. Sci. Comput. 18, 1–22.

Stolar, D.B., G.R., Roe, and S.D., Willett, 2006. Controls on the patterns of topography and erosion rate in a critical orogen. (in submission).

Thackray, G.D., 2001. Extensive early and middle Wisconsin glaciation on the western Olympic Peninsula, Washington, and the variability of Pacific Moisture delivery to the Pacific Northwest. Quat. Res. 55, 257–270.

Tomkin, J.H., Braun, J., 2002. The influence of alpine glaciation on the relief of tectonically active mountain belts. Am. J. Sci. 302, 169–190.

Westbrook, G.K., Ladd, J.W., Buhl, P., Bangs, N., Tiley, G.J., 1988. Cross section of an accretionary wedge; Barbados Ridge Complex. Geology 16, 631–635.

Whipple, K., Tucker, G., 1999. Dynamics of the stream-power river incision model: implications for height limits of mountain ranges, landscape response timescales, and research needs. J. Geophys. Res. 104, 17,661–17,674.

Whipple, K.X., Meade, B.J., 2004. Controls on the strength of coupling among climate, erosion, and deformation in two-sided, frictional orogenic wedges at steady state. J. Geophys. Res. 109. doi:10.1029/2003JF000019.

Whipple, K.X., Meade, B.J., 2006. Orogen response to changes in climatic and tectonic forcing. Earth Planet. Sci. Lett. 243, 218–228.

Willett, S.D., 1999. Orogeny and orography: the effects of erosion on the structure of mountain belts. J. Geophys. Res. 104, 28,957–28,981.

Willett, S., Beaumont, C., Fullsack, P., 1993. Mechanical model for the tectonics of doubly vergent compressional orogens. Geology 21, 371–374.